Dynamic Modeling and Control of Nonholonomic Mobile Robot with Lateral Slip

Naim Sidek and Nilanjan Sarkar Senior *Member, IEEE*

Abstract— **Nonholonomic mobile robots are characterized by no-slip constraints. However, in many practical situations, slips are inevitable. In this work, we develop a theoretical and systematic framework to include slip dynamics into the overall dynamics of the wheeled mobile robot (WMR). Such a dynamic model is useful to understand the slip characteristics during navigation of the WMR. We further design a planner and a controller that allow efficient navigation of the WMR by controlling the slip. Preliminary simulation results are presented to demonstrate the usefulness of the proposed modeling and control techniques.**

Index Terms—**nonholonomic constraint, lateral slip, mobile robot, path following**

I. Introduction

Wheeled mobile robots can be found in many applications such as in transportation, entertainment, planetary exploration, surveillance, mining, and military operations. Majority of WMR platforms currently available in the market do not have omni-directional wheels. They use standard wheels due to the inherent mechanical simplicity. These WMRs are called nonholonomic mobile robots because of their no-slip kinematic constraints. Nonholonomic behavior in robotic systems is particularly interesting because it implies that the mechanism can be controlled with reduced number of actuators.

However, in many practical applications such as outdoor navigation or navigation on a slippery or uneven, irregular surface, the no-slip assumptions are not satisfied. As a matter of fact, slip is required to generate traction force at the contact point that is responsible for the motion of the WMR. It is possible to optimize the traction force and therefore, the maneuverability of the WMR can be improved by controlling the magnitude of the slip as can be seen in car racing [1]. On the other hand, excessive slip may generate instability in motion and thus should be prevented. It can be argued that to improve the previous works on nonholonomic WMRs, which neglect the effect of wheel slips, slip measurement and traction force information must be available in the new system model. In fact, some recent works have incorporated slip variables into the robot model. In [2], the author developed a generalized kinematics model of WMRs that include various slip information namely the side, rolling and turn slips. In [3], slip is treated as small, measurable, bounded perturbation to system states. The friction coefficient is assumed to be very small covering the linear part of traction curve. [4] introduced slip space to develop acceleration slip dynamics of omni-directional WMR and later applied the ideal rolling constraints condition to the design of system controller. In [5], the lateral force control using force and position controllers that include slip factor was discussed. [6] introduced robust controller for trajectory tracking by augmenting the robot kinematics model with slip in the form of transverse function and the stability is confirmed though *Lie* group operation. [7] reported a simpler way to design the navigation controller, whereby having a prior knowledge of terrain characteristic including slip, they generated candidate path for the mobile robot to follow.

The first objective of our work is to develop a theoretical and systematic framework to include slip dynamics into the overall dynamics of the WMR. Such a dynamic model is useful to understand the slip characteristics during navigation of the WMR. We argue that slip information could be effectively utilized to improve the navigation performance of the WMR. In this paper, we further design a planner and a controller that allow efficient navigation of the WMR by controlling the slip. We assume that traction properties of various surfaces are available as in the existing literature [8,9,10], and slip can be measured using various current techniques as reported in [11,12,13,14]. With the terrain types known, *traction curve* can be developed.

The paper is organized as follows. In Section II, we derive the dynamics of the WMR, which includes slip dynamics using *Lagrangian* approach. Section III discusses how traction force can be generated as a function of wheel slip. We develop the planner and controller that allow navigation of the WMR in the presence of slip in Section IV. Section V presents a detailed simulation results to demonstrate the usefulness of the proposed modeling and control techniques.

II. Dynamic Model

A. Model of a nonholonomic WMR

By using the *Lagrange* formulation, the general dynamic equations of a WMR subjected to nonholonomic kinematic constraints can be written in the following form,

$$M(q)\ddot{q} + C(q,\dot{q})\dot{q} = B(q)u + A^T(q)\sigma \qquad (1)$$

$q \in \Re^{n\times 1}$ is a vector of generalized coordinates and $\dot{q} \in \Re^{n\times 1}$ is a vector of longitudinal and angular velocities of

Manuscript received January 18, 2008.

N. Sidek is with the Electrical Engineering Department, Vanderbilt University, Nashville, TN 37235 (615-299-7464; fax: 615-343-6687; e-mail: naim.sidek@vanderbilt.edu).

N. Sarkar is with the Mechanical Engineering Department, Vanderbilt University, Nashville, TN 37235 (e-mail: nilanjan.sarkar@vanderbilt.edu).

978-0-7695-3105-2/08 $25.00 © 2008 IEEE
DOI 10.1109/ICONS.2008.22

generalized coordinates. $M(q) \in \Re^{n \times n}$ is a symmetric positive definite inertia matrix of the system. $C(q,\dot{q}) \in \Re^{n \times n}$ is a centripetal and coriolis forces matrix. $B(q) \in \Re^{n \times (n-m)}$ and $u \in \Re^{(n-m) \times 1}$ are the input transformation matrix and input vector, respectively. $\sigma \in \Re^{m \times 1}$ is a vector of *Lagrange* multipliers and $A^T \sigma$ corresponds to the generalized forces related to the kinematic constraints. The constraints are defined by,

$$A(q)\dot{q} = 0 \tag{2}$$

where $A^T(q) \in \Re^{n \times m}$ is a matrix associated with the kinematic constraints of the nonholonomic system. If $S(q) \in \Re^{n \times (n-m)}$ is defined as a full rank matrix formed by a set of smooth and linearly independent vector fields, spanning the null space of $A^T(q)$, then, $S^T(q)A^T(q) = 0$. Thus, it is possible to find a set of auxiliary vector of time functions,

$$v(t) \in \Re^{(n-m) \times 1}, \quad \forall t, \tag{3}$$

where $\dot{q} = S(q)v(t)$ (4)

$$\dot{v} = \left(S^T M S\right)^{-1} S^T \left(-M\dot{S}v - C + Bu\right) \tag{5}$$

is the acceleration of time vectors . Utilizing (5), proper control laws can be developed, which we discuss in Sect. IV.

***Case study**: A 2-wheeled nonholonomic mobile robot*

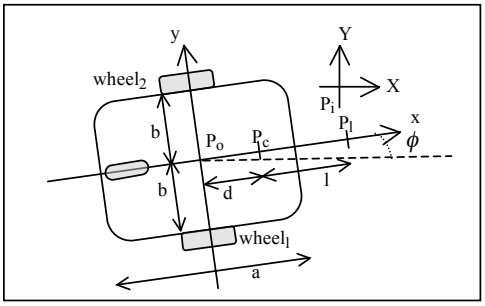

Fig. 1. Nonholonomic WMR platform

The unidirectional platform shown in Fig.1 is a typical example of a nonholonomic WMR. It has two differential driving wheels and a back caster wheel. The two driving wheels are powered by DC motors and have the same wheel radius, *r*. The center of mass (COM) is located at point P_c and P_l is the look-ahead point located on the *x*-axis of the WMR body. Point P_o is the origin of WMR axis, which is located at the intersection of the longitudinal *x*-axis and the lateral *y*-axis. *a* and 2*b* are length and width or WMR body, respectively and *d* denotes the distance between point P_o and point P_c along the *x*-axis. The distance of the look-ahead point is *l* from point P_c also along the *x*-axis. The origin of the inertial frame {*X,Y*} is shown as P_i and as such allows the pose of the WMR to be completely specified through the following vector of generalized coordinates with respect to {*X,Y*},

$$q=[x_c, y_c, \phi, \theta_1, \theta_2]^T \tag{6}$$

where x_c and y_c are the coordinates of the COM. The orientation of the WMR frame from the inertial frame is denoted as ϕ. θ_1, and θ_2 are the angular displacements of driving wheel 1 and wheel 2, respectively. Due to the nonholonomic nature of the system, the constraint equation obeys the ideal no-slip condition. The rolling and the knife-edge constraint equations for this system can be found in [16]. In the next paragraph, these constraints could be relaxed when WMR is subjected to wheel slip.

B. Non-ideal case: A WMR with wheel slippage

In this work we want to investigate the navigation problem of a nonholonomic WMR when the ideal no-slip condition does not hold true. Therefore, we want to include slip into the dynamics of the system. We start by introducing a new slip coordinate vector, $s=[\zeta_1, \zeta_2, \eta_l, \eta_2]^T$. The ζ_1 and ζ_2 are longitudinal slip displacements for wheel 1 and wheel 2, respectively. Likewise, η_l and η_2 are lateral slip displacements. (Note that *s* can be easily extended to a WMR with more wheels). We now augment the set of generalized coordinates to the slip coordinate vector to become,

$$q=[x_c, y_c, \phi, \theta_1, \theta_2, \zeta_1, \zeta_2, \eta_l, \eta_2]^T \tag{7}$$

where $q=\left[q_{l(1\times n)}\ q_{2(1\times s)}\right]^T$ spans the space $\Re^{n+s}$. $q_{l(1\times s)}$ is the original coordinate vector and $q_{2(1\times s)}$ is a vector of slip coordinates. Now, we can introduce slip into the kinematic constraints as follows,

$$\begin{aligned} &\dot{x}_c \cos\phi + \dot{y} \sin\phi + b\dot{\phi} = r\dot{\theta}_1 - \dot{\zeta}_1 \\ &\dot{x}_c \cos\phi + \dot{y} \sin\phi - b\dot{\phi} = r\dot{\theta}_2 - \dot{\zeta}_2 \end{aligned} \tag{8}$$

For the knife-edge/lateral constraints, the two general constraint equations for each wheel are as follows,

$$\begin{aligned} &\dot{y}_c \cos\phi - \dot{x}_c \sin\phi - d\dot{\phi} = \dot{\eta}_l \\ &\dot{y}_c \cos\phi - \dot{x}_c \sin\phi - d\dot{\phi} = \dot{\eta}_2 \end{aligned} \tag{9}$$

$\dot{\zeta}_i$ and $\dot{\eta}_i$ are the longitudinal and lateral slip velocities and for this particular WMR the magnitude of the right-hand terms in (9) are the same due to the nature of the wheels, which are fixed (not steerable). The value, $\dot{\eta}_i$ is also equivalent to the lateral velocity, $\dot{y}_o$ of the WMR body. In this work, we are interested in the agility of WMR navigation and thus concentrate on how the WMR can negotiate sharp turns in the presence of slips. We currently neglect the effect of longitudinal slip and concentrate on lateral slip because it plays an important role during cornering. Now, after we rearrange the coordinate system, the four constraints can be written in the matrix form (2) with $q=[x_c, y_c, , \phi, \eta_l, \eta_2, \theta_1, \theta_2]^T$. We found $A(q)$ to be a full rank matrix and the WMR has three auxiliary time functions, which are chosen as,

$$v = [\dot{\eta}_2, \dot{\theta}_1, \dot{\theta}_2]^T \tag{10}$$

We then construct matrix $S(q)$, which projects matrix $A(q)$ into its null space. Applying *Lagrangian* method to derive the WMR dynamic model using the new generalized coordinates leads to the new dynamic equation of WMR,

$$M(q)\ddot{q} + C(q,\dot{q})\dot{q} + F(q,\dot{q}) = B\tau + A(q)\sigma\ , \tag{11}$$

where $F(q,\dot{q}) = [0,0,0,\textit{traction force}_1, \textit{traction force}_2, 0, 0]^T$, $\tau = [\tau_1, \tau_2]^T$, and *B* is a configuration matrix. The τ_i is the input torque given to each of the motor of the wheels. The

introduction of traction force in the dynamic equation reflects the existence of slips in the dynamics. Now (5) can be rewritten as,

$$\dot{\nu} = \lambda + \kappa\tau \tag{12}$$

where,

$\lambda = \left(S^T MS\right)^{-1} S^T\left(-M\dot{S}\nu - C - F\right)$ and $\kappa = \left(S^T MS\right)^{-1} S^T B\tau$.

III. Traction Force Model

A. Tire/Wheel and Ground Surface Interaction

Besides supporting the weight of the robot and isolating the robot body from the ground surface irregularities, the wheels in a mobile robot provide traction force for mobility. This force depends on the magnitude of longitudinal and lateral slips of the wheel and has varying values on different types of surfaces. In this paper, in order to systematically investigate the effect of wheel slip on WMR navigation, we concentrate on the effects of lateral slip, η_i , alone. Thus to simplify our analysis, the longitudinal slip, ξ_i, is assumed to be under ideal rolling condition. The lateral force, F_y then, can be mathematically related to slip angle, *sa* as follows

$$F_y(sa) = \mu(sa)N \tag{13}$$

where $sa = \tan^{-1}\left(\dot{\eta}/r\dot{\theta}\right)$ and is the measure of angle between the instantaneous velocity of the WMR and the instantaneous velocity of a wheel. μ is the friction coefficient and *N* is the normal force of the WMR.

It is generally difficult to obtain an analytical relationship between the traction force and the slip angle due to several reasons. Previous experimental results in [11], show that the coefficient value is very much dependent on the ground surface types as well as the characteristic of the tire itself. The latter information, i.e., tire characteristics, is generally proprietary and not revealed in detail. As an alternative, an elegant, semi-empirical model based on curve fitting called *Pacejka* model, commonly used in literature [1,14] is used in this research. The equation is given by,

$$F_y = K_1 \sin\left(K_2 \tan^{-1}\left(SK_3 + K_4\left(\tan^{-1}\left(SK_3\right) - SK_3\right)\right)\right) + S_v \tag{14}$$

where all the independent variables, $K_i, i = 1,...,4$, *S*, and S_v are constants and determined by experiments. In Fig. 2, we illustrate two traction forces versus slip characteristics that have been reported in the literature [13] using the above formula. It can be seen from Fig. 2, that the magnitude of traction force varies linearly with the slip angle till the traction force reaches its peak. Once the slip angle exceeds the value corresponding to the peak traction force, the traction force begins to reduce unstably. Meanwhile, the left region of the peak point provides stable, controllable traction force and depending on the control objective can be manipulated to fulfill the mission goal.

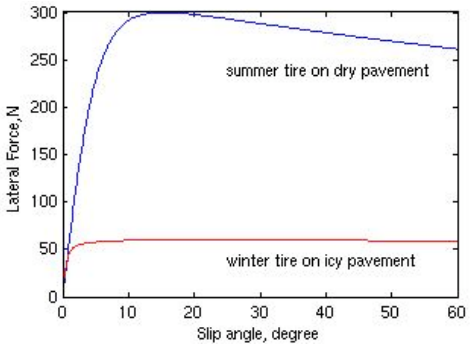

Fig. 2. Lateral Traction Force vs. Slip-angle Relationship

IV. Control and Navigation

A. Output Equations

Output equation is not necessarily and uniquely determined by the state equations of the WMR dynamics system. In fact, the output equations can be chosen in such a way that the tasks to be performed by the WMR can be realistically specified so as the controller design can be developed as simpler as possible without sacrificing the performance.

In this paper, based on the dynamic model previously developed, we approach the problem of WMR navigation under the path following formulation. We refer to Section II for the model and the state equation of the WMR. The coordinate of the look-ahead point P_l is given by,

$$\begin{aligned} x_l &= x_c + l\cos\phi \\ y_l &= y_c + l\sin\phi \end{aligned} \tag{15}$$

By following the conventional wisdom in which one drives a car, we can establish two driving objectives. The first is the WMR has to pursue a given prescribed path as closely as possible and the second is the WMR has to travel the path with a given forward, desired velocity.

Based on the above objectives, we can establish the output equations where, the first equation relates the shortest distance between the WMR (a reference point on the WMR platform) and the desired path. The second equation is to describe the WMR forward velocity. Assuming any path can be realized through a combination of circular and straight segments [15], and let the output equation be denoted by,

$$y = h = \begin{bmatrix} h_1(q) & h_2(q) \end{bmatrix} \tag{16}$$

For a straight-line path, the output equation is,

$$h_1(x_c, y_c, \phi) = \frac{C_1 x_l + C_2 y_l + C_3}{\sqrt{C_1^{\,2} + C_2^{\,2}}}, \tag{17}$$

where C_i, *i*=1,2,3 are constants. From (17), we see the shortest distance can be taken as the absolute value of h_1. By assuming the longitudinal slip to be zero, the forward velocity equation of the WMR is given by,

$$h_2(\nu) = \dot{x}_c\cos\phi + \dot{y}_c\sin\phi = \frac{r}{2}\left(\nu_2 + \nu_3\right) \tag{18}$$

where v_2 and v_3 are the angular velocities of wheel 1 and wheel 2, respectively. The next step is to form the decoupling matrix for feedback linearization as shown below,
where for the straight line,

$$J_{h_1} = \frac{1}{\sqrt{C_1^{\,2} + C_2^{\,2}}}\begin{bmatrix} C_1 & C_2 & C_2 l\cos\phi - C_1 l\sin\phi & 0 & 0 & 0 & 0 \end{bmatrix}$$

and the forward velocity, $J_{h_2} = \begin{bmatrix} 0 & 0 & 0 & 0 & 0 & r/2 & r/2 \end{bmatrix}$.
Thus, the resultant decoupling matrix is,

$$\Phi = \begin{bmatrix} J_{h_1}(q)S(q) \\ J_{h_2} \end{bmatrix}. \tag{19}$$

Utilizing the decoupling matrix, we establish input, output feedback linearization through,

$$\ddot{y} = \begin{bmatrix} \ddot{y}_1 \\ \dot{y}_2 \end{bmatrix} = \begin{bmatrix} \dot{\Phi}v \\ 0 \end{bmatrix} + \begin{bmatrix} \Phi \\ J_{h_2} \end{bmatrix}\dot{v} \tag{20}$$

If we let $u = \dot{v}$ and represent (21) in $\ddot{y} = U + V\dot{v}$, we can use (12) to form,

$$\ddot{y} = U + V\lambda + W\tau \tag{21}$$

where $W = V\kappa$. The relationship between torque and traction force can then be determined directly from the inverse dynamic relationship as given as,

$$\tau = W^{+}\left(u_d - U - V\right), \tag{22}$$

where W^{+} is taken to be the pseudo inverse of W. If we let error, $e = h_{i\_desired} - h_{i\_actual}$,
then the control u can be set to,

$$u = \ddot{y}_{desired} + K_v\dot{e} + K_p e \tag{23}$$

where K_v and K_p are constant gains chosen to ensure the convergence of the control errors. To implement the navigation controller, we model the desired control input using a new function of traction force below,

$$J\left(F_y\right) = \frac{F_{y\max}F_y}{\left(F_{y\max} - F_y\right)^{\mu}} \tag{24}$$

where μ is the decay factor and $F_{y\max}$ is the peak traction force and is uniquely based on the type of ground surfaces. By finding the inverse of (25), we formulate,

$$j\left(F_y\right) = \frac{1}{1 + abs\left(J\left(F_y\right)\right)}, \tag{25}$$

which can behave as a weighted coefficient to the desired forward velocity. From (25), we note the value of the weight approaches one as the traction force gradually moves away from the pre-specified allowable maximum traction, $F_{y\max}$. It converges to zero as it approaches the $F_{y\max}$. The rate of convergence can be set using the decay factor, μ. For a WMR that has maximum velocity capability, $V_{\max}$, we set our desired forward velocity to be,

$$h_{2desired} = j\left(F_y\right)V_{\max} \tag{26}$$

V. Simulations and Analysis

In order to understand how a WMR can navigate in the presence of lateral slip we run a set of computer simulations to verify the validity of the new WMR dynamic model as well as to study the effectiveness of the control strategy presented in Section IV. The WMR parameters are chosen as follows: b=0.75m; d=0.3m; r=0.065m; m_r=30kg; m_w=1kg; I_{ry}=15.625kgm^2; I_{wx}=0.005kgm^2; I_{wy}=0.0025kgm^2. The look-ahead point is chosen to be 1m away from point P_c along the x-axis of WMR body. The gains for the linear feedback loop were designed in such a way that we can get a critically damped output response. The given path has two straight-line segments, connected in perpendicular to form an L-shape path. The idea to have such a shape of path is to see the effect of slip when the WMR is to negotiate a sharp corner simulating a harsh navigation scenario. We present simulation results in three different cases to show how the WMR performs for different desired forward velocities on different surfaces for the L-shaped path. The WMR starts from zero velocity, and the maximum allowable torque for each motor is 20N-m. We use two different surfaces in this study, which was a snowy, slippery surface and a dry, paved surface. The surface properties characterized by the respective traction curves are shown in Fig. 2 in Section III.

***Case 1**: Effect of slip on a snowy, slippery surface and a dry, paved surface when the desired forward velocity is 2m/s.*

In this case, as shown in Fig. 3.1, both simulations of path following problems show that the WMR is able to follow the given path, negotiating the sharp corner in a stable manner.

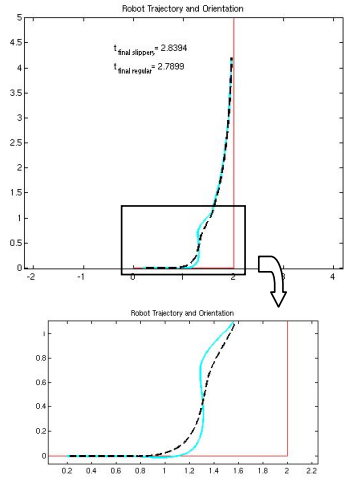

Fig. 3.1. WMR's path following (solid: slippery surface, dash: paved surface)

However, there are differences in path-following performance for the two different ground surfaces. There is a small delay in the WMR response on the slippery surface compare to the regular surface. Consequently, the delay causes the wheel on the slippery surface to take a sharper turn angle (Fig. 3.1). We also observe from the simulation that the WMR takes 0.0494s more time to reach the destination on the slippery surface due to the larger distance error. The dynamic model produced larger lateral slip on the slippery surface due to less traction force as shown in Fig. 3.2. However, even though the slip on the regular surface is approximately 1/10th of the slippery

surface, the available traction force is much bigger as shown in Fig. 3.3b.

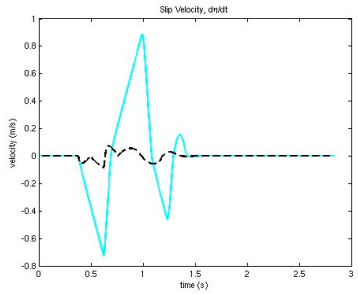

Fig. 3.2. Slip velocity (solid: slippery surface, dash: regular surface)

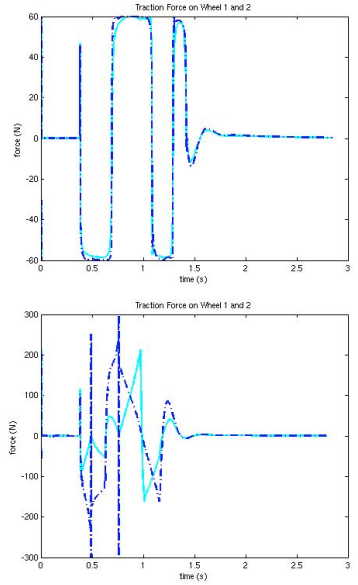

Fig. 3.3. Traction force slippery surface (top) and regular surface (bottom) (solid: wheel1, dash: wheel2)

Case 2*: Effect of slip on a snowy slippery surface and a dry, paved surface when the desired forward velocity is 3.5m/s*

In *case 2* we increase the desired forward velocity to investigate the effect of lateral slip on WMR navigation. It is clear from Fig. 4.1 that the WMR on slippery surface slips from the prescribed path uncontrollably. Fig. 4.2 shows that the corresponding lateral slip for the WMR on the slippery surface grows bigger and as a result of that Fig. 4.3 reveals the sign of instability. Notice that the time period, T, which is measured from the time when the traction curve reaches its peak at $60N$ (Fig. 2) and stays in the vicinity of the peak value, denotes the time spent by wheel 1 (of the WMR) in the unstable region of traction curve in Fig. 2. We observe that the increase in the magnitude of T in the subsequent cycles of the traction force *vs*. time signal can be related to the instability in the path following problem. As a result, there is a need to reduce this time period so that the WMR can be stabilized to follow the path.

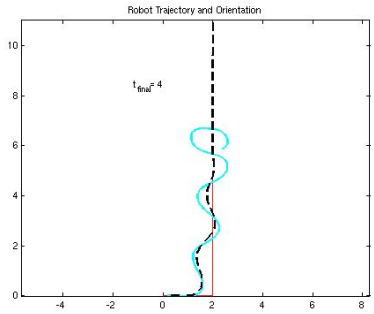

Fig. 4.1. WMR's path following (solid: slippery surface, dash: regular surface)

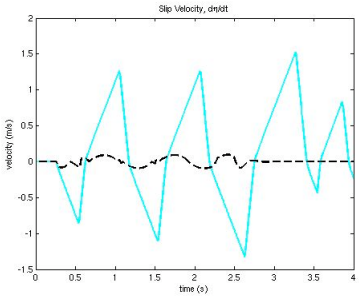

Fig. 4.2. Slip velocity (solid: slippery surface, dash: regular surface)

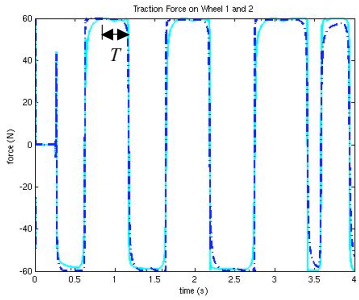

Fig. 4.3. Traction force for slippery surface (solid: wheel1, dash: wheel2)

Case 3*: Effect of a planning strategy to control the slip on both a slippery (snowy) surface and a dry, regular (paved road) surface by autonomous adaptation of the desired forward velocity (max 3.5m/s)*

In *Case 3*, we show that by using the navigation controller developed in (25), we can adaptively change the desired forward velocity based on the available traction force and thus can stabilize the WMR during path-following at high-speed. In particular, we have seen in *Case 2* that the WMR becomes unstable on the slippery surface. In this case, we show by adaptively changing the desired forward velocity during cornering, the WMR can still be made to follow the path at the desired velocity on the slippery surface. Fig. 5.1 shows that the WMR can follow the path in a stable manner and the distance error is reduced to zero (Fig. 5.2b). From Fig. 5.2a, we see that the desired velocity is gradually reduced at the rate of $0.2 m/s^2$ and $0.5\ m/s^2$ for the WMR on regular and slippery

surfaces, respectively and then eventually reach the 3.5*m/s* velocity.

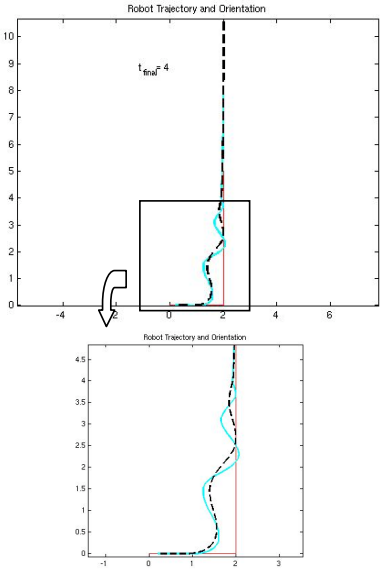

Fig. 5.1. WMR's path following (solid: slippery surface, dash: regular surface)

The instantaneous magnitude of the reduced velocity is slightly bigger for the slippery surface compared to the regular surface so as to shorten the period in which the traction force is in the unstable region as shown in Fig. 5.3.

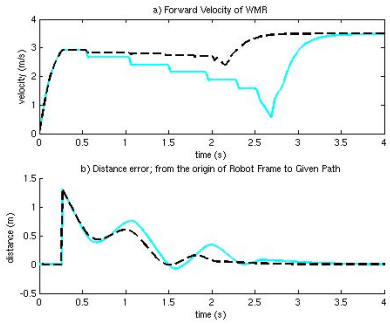

Fig. 5.2. a). Forward velocity, b). Distance error (solid: slippery surface, dash: regular surface)

IV. CONCLUSION

In this paper, we have investigated how a WMR navigates in the presence of lateral slip. We model the WMR in such a way that the wheel/ground contact points allow lateral slip. In order to include the slip into the WMR dynamics we have included the slip coordinates into the set of the original generalized coordinates used to model a nonholonomic WMR. A nonlinear feedback controller is designed to develop the relationship between the dynamic torque value given to the motor and the available traction force. Furthermore, a dynamic planner is designed that allows stable path-following navigation of the WMR with controlled lateral slip. Extensive simulations have been performed to illustrate the usefulness of the presented dynamic model, the planner, and the controller for WMR navigation. In the future work, we plan to implement these ideas into Pioneer P3 robot. We also want to introduce longitudinal slip along with lateral slip to further understand WMR navigation in the presence of slips.

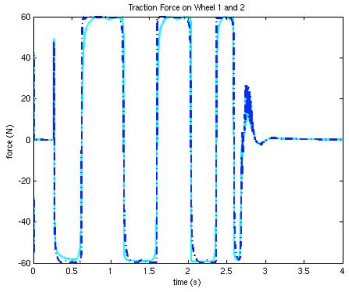

Fig. 5.3. Traction force for slippery surface (solid: wheel1, dash: wheel2)

REFERENCES

[1] http://www.racer.nl/reference/pacejka.htm

[2] M. Tarokh, G.J. McDermott, "Kinematics modeling and analyses of articulated rover",*IEEE Trans. Robotics*, vol.21,no.4, pp.539-553, 2005

[3] I. Motte, G.A. Campion, "Slow manifold approach for the control of mobile robots not satisfying the kinematic constraints", *IEEE Trans. on Robotics and Automation*, vol. 16, no. 6, pp. 875-880, 2000

[4] D. Stonier, C. Se-Hyoung, C. Sung-Lok, N.S. Kuppuswamy, K. Jong-Hwan, "Nonlinear slip dynamics for an omniwheel mobile robot platform", *IEEE International Conference on Robotics and Automation,* pp. 2367 – 2372, April 2007

[5] S. Jung, T.C. Hsia, "Explicit lateral force control of an autonomous mobile robot with slip", *EEE/RSJ Int. Conf. on Intelligent Robots and Systems, IROS 2005*, pp. 388 – 393, 2005

[6] X. Zhu, G. Dong, D. Hu, Z. Cai, "Robust tracking control of wheeled mobile robots not satisfying nonholonomic constraints", *Proc. of the 6th Int. Conf. on Intelligent Systems Design and Applications,* 2006

[7] G. Ishigami, K. Nagatani, K.Yoshida, "Path planning for planetary exploration rovers and its evaluation based on wheel slip dynamics", *Proc. of IEEE Int. Conf. on Robotics and Automation,* 2007

[8] N. Vandapel, D.F. Huber, A. Kapuria, M. Hebert, "Natural terrain classification using 3-D ladar data", *Proc. of IEEE Int. Conf. on Robotics and Automation*, vol. 26 , pp. 5117 – 5122, 2004

[9] C. Weiss, H. Frohlich, A. Zell, "Vibration-based terrain classification using support vector machines", *IEEE/RSJ Int. Conference on Intelligent Robots and Systems*, pp. 4429 – 4434, 2006

[10] C. A. Brooks, K. Iagnemma, "Vibration-based terrain classification for planetary exploration rovers", *IEEE Transactions on Robotics and Automation,* vol. 21, no. 6, pp. 1185 – 1191, 2005

[11] L. Li, F.Y. Wang, "Integrated Longitudinal and lateral tire/road friction modeling and monitoring for vehicle motion control", *IEEE Trans. Intelligent Transportation Sys*, vol.7, no.1, pp.1-19, 2006

[12] C. C. Ward, K. Iagnemma, "Model-Based Wheel Slip Detection for Outdoor Mobile Robots", *IEEE International Conference on Robotics and Automation,* pp. 2724 – 2729, 2007

[13] A. Angelova, L. Matthies, L., D.M. Helmick, G. Sibley, P. Perona, "Learning to predict slip for ground robots*", Proc. of IEEE Int. Conf. on Robotics and Automation*, pp. 3324-3331, 2006

[14] G. Baffet, A. Charara, J. Stephant, "Sideslip angle, lateral force and road fricion estimation in simulations and experiments",*Proc. of IEEE Int. Conf. on Control Applications,* pp. 903-908, 2006

[15] L.E. Dubins, " On curves of minimal length with a constraint on average curvature, and with prescribed initial and terminal positions and tangents", *American Journal of Mathematics*, vol. 79, pp. 497-516, 1957

[16] X. Yun, N. Sarkar, "Unified formulation of robotic systems with holonomic and nonholonomic constraints", *IEEE Transactions on Robotics and Automation,* vol. 14, no. 4, pp. 640 – 650, 1998